CHEMICAL ENGINEERING TRANSACTIONS
VOL. 57, 2017
A publication of AIDIC
The Italian Association of Chemical Engineering
Online at www.aidic.it/cet
Guest Editors: Sauro Pierucci, Jiří Jaromír Klemeš, Laura Piazza, Serafim Bakalis

ISBN 978-88-95608- 48-8; **ISSN** 2283-9216

Supercritical Antisolvent Process to Produce Cerium Oxide Nanoparticles as a Support for High-Activity Platinum Catalysts

Vincenzo Palma, Arianna Pietrosanto, Marco Martino, Ernesto Reverchon, Iolanda De Marco*

University of Salerno, Department of Industrial Engineering, Via Giovanni Paolo II, 132, 84084, Fisciano (SA), Italy]
idemarco@unisa.it

Cerium acetylacetonate ($Ce(acac)_3$) was precipitated from methanol (MeOH) using supercritical antisolvent process (SAS). The precursor was, then, calcined obtaining the cerium oxide (CeO_2). Platinum (Pt) supported on cerium oxide is active for the water gas shift reaction, showing higher activity if compared with platinum supported on other oxides. The catalyst based on platinum supported on cerium oxide obtained using SAS process is more active than the Pt/CeO_2 catalyst obtained in a conventional manner. The precursor nanoparticles were precipitated at different pressures and concentrations of the $Ce(acac)_3$/MeOH solution. At the best operating conditions, nanoparticles with a diameter in the range 40-65 nm were obtained. The catalytic activity and the selectivity of two different samples was studied and compared. The catalysts were characterized by X-ray diffraction, field emission scanning electron microscopy, infrared spectroscopy, nitrogen adsorption and desorption at 77 K, and mercury porosimetry.

1. Introduction

Water gas shift reaction (WGS) ($CO + H_2O \leftrightarrows CO_2 + H_2$, $\Delta H = -41.1$ kJ mol^{-1}) is important in the increasing of H_2 yield in syngas and has an important role in the production of chemicals, such as methanol and ammonia, because it provides H_2/CO mixtures with an appropriate ratio (Twigg and Dupont, 2014). Moreover, in the plants where high-purity H_2 for fuel cells are produced, the conversion of CO to obtain H_2 rich streams is strongly encouraged because it does not consume energy, and delivers additional fuel (Brunetti et al., 2007). WGS is a reversible and exothermic reaction. The reaction is thermodynamically favored at low temperature and kinetically favored at high temperature. Therefore, the conventional WGS has two process stages in industrial applications: (1) high-temperature shift (HTS) carried out in the temperature range 623–873 K and (2) low-temperature shift (LTS) carried out in the temperature range 453–633 K. The catalysts most commonly used for HTS and LTS are iron-chromium-based catalyst (Fe-Cr) and copper-zinc-based catalyst (Cu-Zn), respectively (Chu et al., 2015). The traditional two-stage WGS is very effective; indeed, can reduce CO to a few thousands of ppm or lower. However, researchers are laboring to simplify the complex multi-steps process, because it shows some disadvantages, such as the slow kinetics at lower temperatures, which requires a high mass of catalyst the presence of an inter-cooling stage, which increases energy requirements (and, therefore, the environmental impact of the process), the plant cost (Palma et al., 2009) and the limitation of thermodynamic conversion at higher temperatures. For these reasons, a single stage WGS seems a solution for the simultaneous reduction of reactor dimensions and of the productions costs (Palma et al., 2016). Therefore, it is important the choice of a good catalytic formulation.
In the last years, different studies on noble metal based catalysts; i.e., Gold (Yang et a., 2013), Platinum (Franchini et al., 2012), Rhodium (Cornaglia et al., 2012), Palladium and Rutenium (Mierczynski et al., 2013) were performed, because, they have a very high compatibility with a fuel processor system; moreover, even at low concentrations, they show high H_2 yields in a wide range of temperatures. Among these catalysts, the best performances were obtained using Platinum and Gold. In particular, Gold based catalysts show the higher activity for LTS, but, unfortunately, sintering phenomena occur, which cause the rapid deactivation of the

catalyst. The anchorage of the active phase to the support can be obtained only using complex strategies (Ta et al., 2012). For these reasons, a good solution to obtain catalysts highly active and stable at the same time is the preparation of Platinum based catalysts (Palma et al., 2014).
Platinum based catalysts are frequently supported on reducible oxides, prepared in different ways. For example, Pt/CeO_2 nanofibers with diameter in the range 80−120 nm, with a good CO conversion in the temperature range 593−633 K, were obtained by Tang et al. (2012) using electrospinning. Kyung-Ran et al. (2013) added titanium to Pt/ZrO_2 to increase the support surface area and the Pt dispersion, obtaining an enhancement of the catalyst reducibility and a faster decomposition rate of the intemediate. Among the different reducible oxides, CeO_2 has been supported on Platinum based catalysts also in other kind of reaction. For example, good results were obtained using CeO_2-Pt-Ni and CeO_2-Pt-Co catalysts in the low temperature bio-ethanol steam reforming (Palma et al., 2011). A way to improve the activity of the catalyst is he use of nanocrystalline oxide supports, such as nanoparticles, instead of larger crystallites (Carretin et al., 2004). Among the innovative techniques used to obtain nanoparticles, good results can be obtained using supercritical fluids based processes.
In particular, supercritical carbon dioxide ($scCO_2$) is widely used because it is inexpensive, non-toxic and can be easily separated from products and organic solvents used during the processes (Prosapio et al., 2014). $scCO_2$ is characterized by fast mass transfer, high solvent power, high density, near zero surface tension, low viscosity and high diffusivity, that can be tuned varying pressure and temperature (Cardea et al., 2013). In this work, nanocrystalline CeO_2 was prepared using supercritical antisolvent process (SAS), which revealed to be a good technique to obtain both microparticles and nanoparticles (De Marco et al., 2015). An important result obtainable using this process is that the attainment of nanoparticles and their separation are conducted in one-step process (Torino et al., 2010). SAS process is based on two pre-requisites: $scCO_2$ has to be completely miscible with the liquid solvent; whereas, the solute has be insoluble in the mixture solvent/$scCO_2$. $scCO_2$ very fast diffusion (the diffusivity of $scCO_2$ is about two orders of magnitude larger than that of conventional liquids) into the liquid solvent produces the supersaturation of the solute and its precipitation in micronized particles down to particle diameters that are not possible to obtain using liquid antisolvents or by other techniques like jet milling. The control of the particle size distribution (PSD) is also possible. In this paper, Cerium acetylacetonate ($Ce(acac)_3$) was precipitated from methanol (MeOH) using the SAS process and then calcined obtaining CeO_2 nanoparticles. Pt was supported on nanocrystalline CeO_2 obtained by SAS (PtCeSAS) and on commercial CeO_2 nanoparticles (PtCeComm). WGS was conducted using both the supports and the CO conversions and H_2 selectivities were compared.

2. Materials and methods

2.1 Preparation of CeO_2

$Ce(acac)_3$ was provided by Strem Chemicals, commercial CeO_2 nanoparticles, MeOH and Tetraammineplatinum (II) nitrate $[Pt(NH_3)_4](NO_3)_2$ were supplied by Sigma–Aldrich. CO_2 (purity 99%) was purchased from S.O.N. s.p.a. All materials were used as received. A scheme of the SAS apparatus used to obtain CeO_2 from $Ce(acac)_3$ is reported in Figure 1. The plant mainly consists of two pumps used to deliver the liquid solution and $scCO_2$, respectively. A cylindrical vessel is used as precipitation chamber. The liquid mixture is delivered to the precipitator through a stainless steel nozzle, whereas $scCO_2$ is co-current delivered through another port to the chamber. The temperature is assured by a PID controller connected with electrically thin heating bands and the pressure in the chamber is measured using a test gauge manometer and regulated by a micrometric valve. A stainless steel frit (pore diameter of 0.1 μm) located at the bottom of the chamber is used to collect the produced powder. A second vessel located downstream the micrometric valve, which pressure is regulated by a backpressure valve, is used to recover the liquid solvent. At the exit of the second vessel, the CO_2 flow rate is measured by a rotameter. A SAS experiment usually begins delivering CO_2 to the SAS vessel until the desired pressure is reached. When antisolvent steady flow is established, the mixture of organic solvents is sent through the nozzle to the chamber for at least 15 min. When a quasi-steady state composition of solvents and antisolvent is realized inside the SAS vessel, the flow of the solvents is stopped and the liquid solution is delivered through the nozzle, producing the precipitation of the solute. At the end of the solution delivery, supercritical CO_2 continues to flow, to wash the chamber, eliminating the solution formed by the liquid solubilized in the supercritical antisolvent. At the end of the washing step, CO_2 flow is stopped and the precipitator is depressurized down to atmospheric pressure. The range of the operating conditions chosen to obtain $Ce(acac)_3$ nanoparticles were: pressure equal to 20 MPa; temperature equal to 313 K; liquid solution prepared at 4–8 mg/mL MeOH and pumped at 1–2 mL/min; carbon dioxide molar fraction equal to 0.98. The precursor was recovered and calcined at 673 K for 2 h.

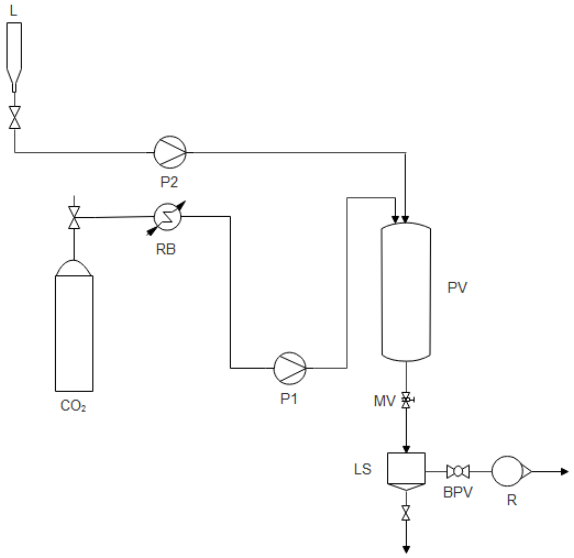

Figure 1: Schematic representation of SAS apparatus. CO_2: CO_2 supply; L: liquid solution; RB: refrigerating bath; P1, P2: pumps; PV: precipitation vessel; MV: micrometering valve; LS: liquid separator; BPV: back-pressure valve; R: rotameter.

2.2 Catalysts preparation

The 1 % Pt/CeO_2 SAS (PtCeSAS) and 1 % Pt/CeO_2 commercial (PtCeComm) catalysts, both containing 1 %w/w of Platinum, were prepared by impregnation of the support with an aqueous solution of the proper amount of $[Pt(NH_3)_4](NO_3)_2$, and the mixture was stirred at the boiling point until evaporation occurred. The resulting solid was dried in an oven at 393 K for 2 h and then calcined at 673 K for 2 h.

2.3 Catalysts characterization

Samples of the precipitated material were observed by a Field Emission Scanning Electron Microscope (FESEM, mod. LEO 1525,Carl Zeiss SMT AG). Powder was dispersed on a carbon tab previously stuck to an aluminium stub (Agar Scientific); then, was coated with Gold using a sputter coater (mod. 108A, Agar Scientific).
Fourier transform infrared (FT–IR) spectra were obtained via M2000 FTIR (MIDAC Co), at a resolution of 0.5 cm^{-1}. The scan wavenumber range was 4000–450 cm^{-1}, and 16 scan signals were averaged to reduce the noise. The powder samples were ground and mixed thoroughly with potassium bromide (KBr) as infrared transparent matrix. KBr discs were prepared by compressing the powders in a hydraulic press. Specific surface area was determined by nitrogen adsorption-desorption isotherms at 77 K using the Brunauer, Emmet and Teller (BET) equation (Quantachrome Instruments, mod. Nova 1200e). Prior to the measurement, about 200 mg of the sample was heated at 443 K for 2 h under vacuum. For the determination of the surface area, adsorption isotherms in the linear region of the BET plot (at a relative pressure p/p0 in the range 0.05–0.3) using a multipoint BET were determined. The effective metal loading of the catalysts was determined through the Energy Dispersive X-ray fluorescence (EDXRF) spectroscopy (Thermo-Scientific Quant'X). The powder XRD patterns (Cu Kα radiation) were recorded by a D8-Advance Bruker WAXRD spectrometer, and the crystallites size was determined. The Raman spectra were obtained by a Renishaw inVia microRaman spectrometer (514 nm excitation wavelength). The thermogravimetric analysis (TGA) was performed by a Q600 connected to a quadrupole- mass spectrometer detector Discovery MS TA Instruments. The temperature programmed reduction (TPR) was carried out on 3 cm^3 of samples in powder form, performed in a tubular stainless steel reactor (internal diameter of 22 mm). A 5 % H_2/N_2 gas mixture (flow rate: 500 Ncm^3/min) was fed to the reactor, and temperature was raised up to 673 K with a heating rate of 10 K/min. The hydrogen uptake was recorded by an online ABB system equipped with a thermal conductivity detector ''Caldos 17" for H_2.

2.4 WGS experimental tests

The Water Gas Shift tests were performed at atmospheric pressure, in a temperature range of 493-643 K. The reacting mixture consisted of 8 % CO, 24 % H_2O and Nitrogen balance. The activity of the catalysts was tested in a fixed bed tubular stainless steel reactor having an internal diameter of 22 mm. All the samples were crushed into powder and sieved (180-355 μm) to reach 3 cm^3 of catalyst (the size of the particles are the optimal ones to avoid the limitations to mass transfer), diluted 1:1 vol with quartz (180-355 μm), in order to

minimize the pressure drops and the thermal effect of the exothermic reaction. These dimensions of quartz particles guarantee the optimal distribution of the catalyst along the bed to avoid packing phenomena. The gas hourly space velocity (GHSV) was set up to 5,000 h^{-1}. All the catalysts were reduced by TPR before reaction. Products stream was continuously analyzed by a ABB system equipped with an infrared detector ''Uras 14" for CO, CO_2 and CH_4, and a thermal conductivity detector ''Caldos 17" for H_2.

3. Results and discussion

3.1 Characterization

Among the different operating conditions tested to obtain the nanocrystalline $Ce(acac)_3$, the best ones in terms of dimensions and productivity were: flow rate equal to 2 mL/min and concentration of the liquid solution equal to 6 mg/mL. The FESEM image of the nanoparticles obtained in these conditions (with a diameter equal to 50±20 nm) is reported in Figure 2a, whereas, in Figures 2b, 2c and 2d, the FESEM images of the CeO_2 SAS powder, PtCeSAS and PtCeComm catalysts are shown. The catalysts were subjected to X-ray diffraction analysis (reported in Figure 3) and the results were compared. Indeed, the enlargement of the peaks shows the crystallites' nanometric dimensions; in particular, as the crystallites dimensions reduced, the peaks enlarged. The support crystallites size of the catalysts were determined from X-ray line broadening using the Scherrer. In Table 1, the main results of the characterization of the CeO_2 and of the catalysts were reported. The specific surface areas recorded for all samples showed that the addition of the Pt involve an increase of the specific surface area.

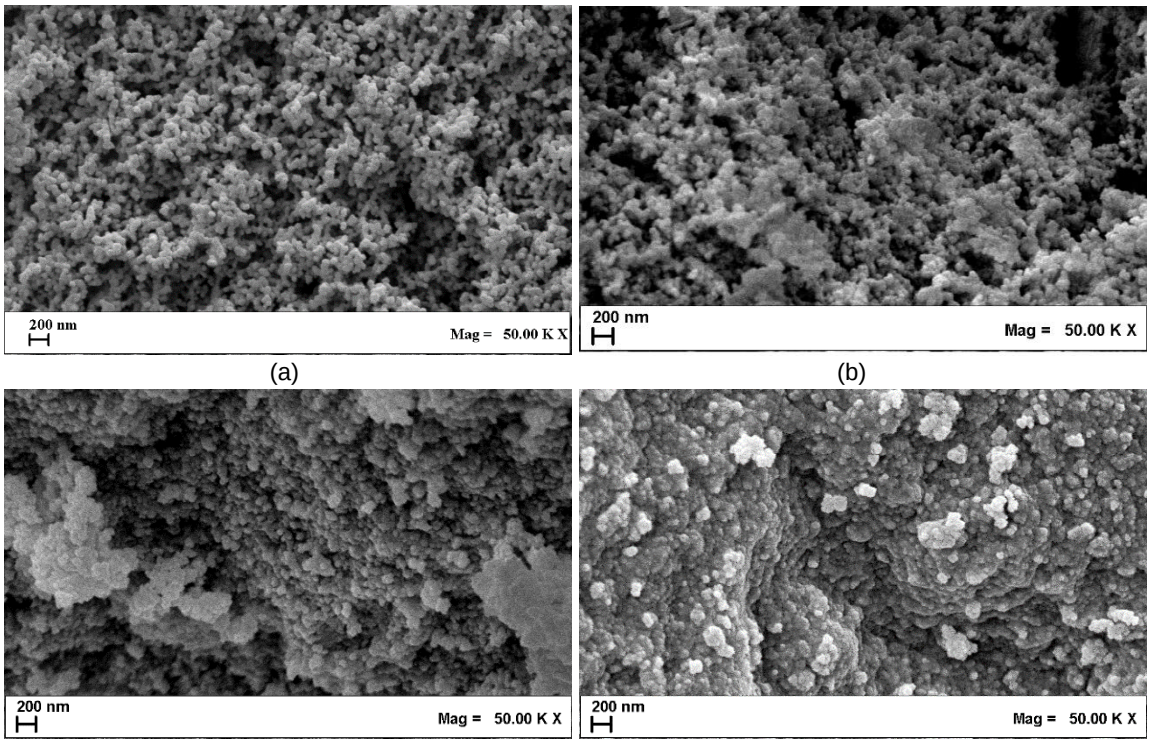

Figure 2: FESEM images of (a) $Ce(acac)_3$ SAS (b) CeO_2 SAS (c) PtCeSAS and (d) PtCeComm.

Table 1: CeO_2 nanoparticles and catalysts characterization: Specific Surface Area, average crystallite size, EDXRF Pt content, TPR H_2 uptake

Sample	B.E.T., m^2/g	Cryst. Size, nm	Pt load. % w/w	H_2 uptake, mmol/g
CeO_2 SAS	44	12	-	-
CeO_2 comm	56	42	-	-
PtCeSAS	75	14	0.93	0.014
PtCeComm	64	42	0.73	0.016

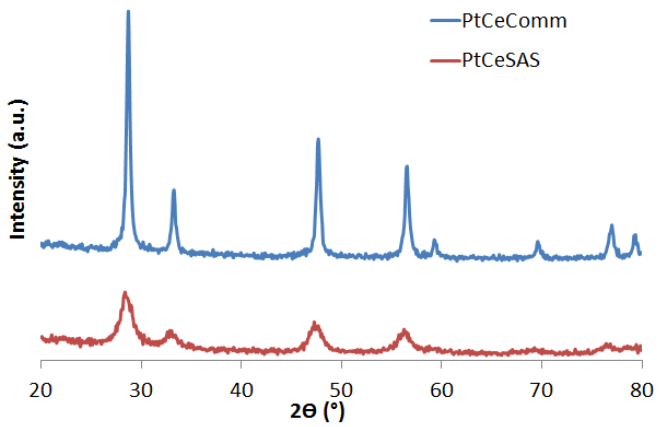

Figure 3: XRD of PtCeSAS and PtCeComm.

Results in Table 1 and Figure 3 clearly show that the crystallite size of the SAS CeO_2 nanoparticles is lower than the commercial CeO_2 nanoparticles both before and after the deposition of the active phase.

3.2 Activity and selectivity WGS test

The catalytic activity results are summarized in Figure 4, in terms of CO conversion and H_2 yield as functions of temperature in the range 520–620 K. The activity data at each temperature were determined after stabilization of the concentration of the species, and no deactivation was detected during the tests. As it is possible to observe from the figure, the CO conversion increases with the temperature; at temperatures higher than 580 K the two catalysts are in very good agreement with the equilibrium calculations, with a conversion higher than 98 %. At lower temperatures, it is possible to note that the PtCeSAS catalyst leaves the equilibrium at 553 K, whereas the PtCeComm catalyst leaves the equilibrium at 563 K. In particular, at 531 K, the PtCeComm catalyst reached a conversion of 81%, while the PtCeSAS showed a conversion of 89%, corresponding to CO residual concentrations of about 15200 and 8800 ppm respectively. Also the H_2 yield increases with the temperature, and also for this parameter the PtCeSAS sample showed better results, whereas at lower temperatures, the values of H_2 selectivity are comparable.

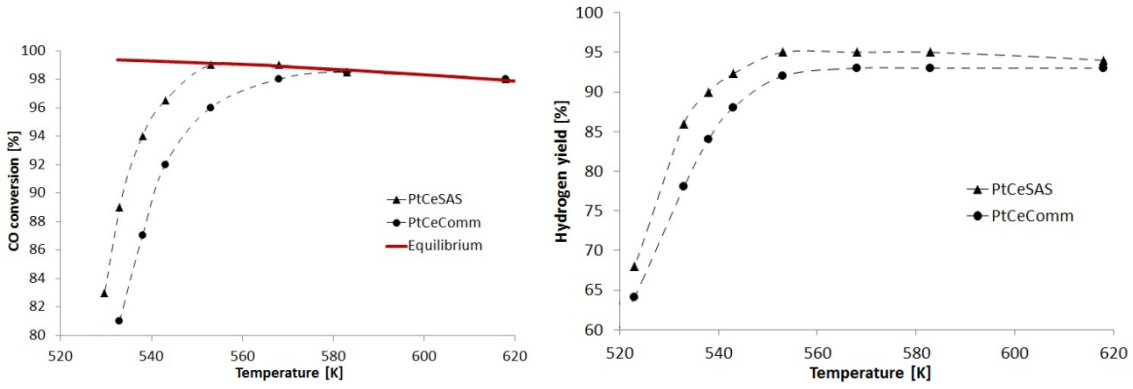

Figure 4: Pt/CeO_2 X_{CO} vs T (left); H_2 selectivity vs T (right).

4. Conclusions

In this work, we demonstrated that it was possible to obtain ceria nanoparticles, characterized by very good performances as catalyst support. Pt based catalyst supported on ceria nanoparticles obtained through a supercritical antisolvent process was prepared and the catalytic performances were compared with a catalyst prepared using commercial ceria nanoparticles. The PtCeSAS catalyst shows a higher specific surface area and smaller crystallites. As a consequence, the CO conversion, and the H_2 yield at lower temperature are sensibly higher for the PtCeSAS catalyst, confirming the beneficial role of the proposed technique for the preparation of cerium oxide nanoparticles as support for improved activity Pt based catalysts.

Acknowledgments

The authors acknowledge Dr. Paola Franco for her help in performing the experiments. The financial support of MIUR (Italian Ministry of Scientific Research) is also acknowledged.

References

Brunetti A., Caravella A., Barbieri G., Drioli E., 2007, Effect of membrane selectivities on WGS reaction in a nonisothermal membrane reactor, Chemical Engineering Transactions, 11, 449–454.

Cardea S., Baldino L., De Marco I., Pisanti P., Reverchon E., 2013, Supercritical gel drying of polymeric hydrogels for tissue engineering applications. Chemical Engineering Transactions, 32, 1123–1128.

Carretin S., Conception P., Corma A., Lopez Mieto J.M., Puntes V.F., 2004, Nanocrystalline CeO_2 Increases the Activity of Au for CO Oxidation by Two Orders of Magnitude, Angewandte Chemie International Edition,43, 2538–2540.

Chu H., Li Q., Meng A., Zhang Y., 2015, Investigation of hydrogen production from model bio-syngas with high CO_2 content by water-gas shift reaction, International Journal of Hydrogen Energy, 40(11), 4092–4100.

Cornaglia C.A., Múnera J.F., Cornaglia L.M., Lombardo E.A., Ruiz P., Karelovic A., 2012, Effect of the support on the catalytic stability of Rh formulations for the water–gas shift reaction, Applied Catalysis A: General, 435–436, 99–106.

De Marco I., Rossmann M., Prosapio V., Reverchon E., Braeuer A., 2015, Control of particle size, at micrometric and nanometric range, using supercritical antisolvent precipitation from solvent mixtures: Application to PVP, Chemical Engineering Journal, 273, 344–352.

Franchini C.A., Duarte de Farias A.M., Albuquerque E.M., dos Santos R., Fraga M.A., 2012, Single-stage medium temperature water-gas shift reaction over Pt/ZrO2-Support structural polymorphism and catalyst deactivation, Applied Catalysis B: Environmental, 117–118, 302–309.

Kyung-Ran H., Son-Ki I., Soon-Chul P., Jong-Soo P., 2013, Pt/ZrO_2 catalyst for a single-stage water-gas shift reaction: Ti addition effect, International Journal of Hydrogen Energy, 38, 6044–6051.

Mierczynski P., Maniukiewicz W., Maniecki T.P., 2013, Comparative studies of Pd, Ru, Ni, $Cu/ZnAl_2O_4$ catalysts for the water gas shift reaction, Central European Journal of Chemistry, 11, 912–919.

Palma V., Palo E., Ciambelli P., 2009, Structured catalytic substrates with radial configurations for the intensification of the WGS stage in H_2 production, Catalysis Today, 147, S107–S112.

Palma V., Palo E., Castaldo F., Ciambelli P., Iaquaniello G., 2011, Catalytic activity of CeO_2 supported Pt-Ni and Pt-Co catalysts in the low temperature bio-ethanol steam reforming, Chemical Engineering Transactions, 25, 947–952.

Palma V., Pisano D., Martino M., Ricca A., Ciambelli P., 2014, Comparative studies of low temperature water gas shift reaction over platinum based catalysts, Chemical Engineering Transactions, 39, 31–36.

Palma V., Pisano D., Martino M., Ciambelli P., 2016, Structured catalysts with high thermoconductive properties for the intensification of Water Gas Shift process, Chemical Engineering Journal, 304, 544–551.

Prosapio V., Reverchon E., De Marco I., 2014, Antisolvent micronization of BSA using supercritical mixtures carbon dioxide + organic solvent, The Journal of Supercritical Fluids, 94, 189–197.

Ta N., Liu J., Chenna S., Crozier P.A., Li Y., Chen A., Shen W., 2012, Stabilized Gold Nanoparticles on Ceria Nanorods by Strong Interfacial Anchoring, Journal of the American Chemical Society, 134, 20585–20588.

Tang H., Sun H., Chen D., Jiao X., 2012, Fabrication of Pt/CeO_2 nanofibers for use in water–gas shift reaction, Materials Letters, 77, 7–9.

Torino E., De Marco I., Reverchon E., 2010, Organic nanoparticles recovery in supercritical antisolvent precipitation, The Journal of Supercritical Fluids, 55, 300–306.

Twigg M.V., Dupont V., 2014, Hydrogen production from fossil fuel and biomass feedstocks, in Advances in Hydrogen Production, Storage and Distribution, 43–84.

Yang Mi., Allard L.F., Fleytzani-Stephanopoulos M., 2013, Atomically Dispersed Au-(OH)x Species Bound on Titania Catalyze the Low-Temperature Water-Gas Shift Reaction, Journal of the American Chemical Society, 135, 3768–3771.